Available online at www.sciencedirect.com
ScienceDirect
Surface & Coatings Technology 201 (2006) 1685–1694
SURFACE & COATINGS TECHNOLOGY
www.elsevier.com/locate/surfcoat

Oxidation studies of CrAlON nanolayered coatings on steel plates

A. Kayani [a,*], R.J. Smith [a], S. Teintze [a], M. Kopczyk [a], P.E. Gannon [a], M.C. Deibert [a], V.I. Gorokhovsky [b], V. Shutthanandan [c]

[a] Department of Physics, Montana State University, Bozeman, MT 59715, United States
[b] Arcomac Surface Engineering, LLC., Bozeman, MT, United States
[c] Pacific Northwest National Laboratory, Richland, WA, United States

Received 27 May 2005; accepted in revised form 25 February 2006
Available online 27 April 2006

Abstract

The requirements of low cost and high-temperature corrosion resistance for bipolar interconnect plates in solid oxide fuel cell stacks have directed attention to the use of metal plates with oxidation resistant coatings. We have investigated the performance of steel plates with nanolayered coatings consisting of $[CrON/AlON]_n$. The coatings were deposited using large-area filtered arc deposition technology, with various O/N pressure ratios, and subsequently annealed in air for up to 25 h at 800 °C. The composition, structure and surface morphology of the coated plates were characterized using RBS, nuclear reaction analysis, and AFM techniques. By altering the architecture and composition of the coatings, the rate of oxidation was reduced relative to the uncoated steel plates, and Fe diffusion from the substrate to the surface through the coating was significantly reduced.

Keywords: CrAlON; Oxynitride; Interconnect; Coatings; Ion beam analysis; Corrosion resistance

1. Introduction

Solid oxide fuel cells (SOFC) are becoming increasingly attractive as a way of transforming chemical energy into electrical energy by means of the electrochemical combination of hydrogen and oxygen via an ion-conducting solid oxide electrolyte. The operational requirements of high ionic conductivity and good catalytic performance in the fuel cell must be balanced against the practical requirements of low cost and high-temperature corrosion resistance for components in the fuel cell stack [1]. Of particular interest in our work is the bipolar plate serving as the current collector or interconnect between adjacent cells of the SOFC stack. The interconnect must not only retain low electrical resistivity throughout the operating lifetime of the fuel cell, but must also have good surface stability and compatibility with thermal expansion properties of the materials in the stack [2]. Doped $LaCrO_3$ plates have worked well for cells operating at 1000 °C, but suffer from high cost as well as difficulties in fabrication. The recent trend towards lower operating temperatures (500–750 °C) may enable the use of more cost-effective materials for the current collector. A thorough evaluation of several heat-resistant alloys with a variety of compositions led to the conclusion that it would be difficult for most traditional alloys to meet the materials requirements of long-term operation above 700 °C [3]. Alloys of body centered cubic, ferritic stainless steels appear to have thermal expansion coefficients that are well matched to other components in the stack, but do not have a sufficiently high electrical conductivity for the desired operating lifetime. The authors conclude that for improved oxidation resistance and electrical conductivity either new alloys will need to be developed, or surface engineering of existing alloys will be required [3]. Among candidate materials in the former category is Crofer22 APU, an Fe–Cr based ferritic stainless steel containing additional manganese, available from ThyssenKrupp VDM [4]. The present work falls into the latter category of surface engineering, namely, the use of coatings to improve oxidation resistance while maintaining acceptably low resistivity values. The use of coatings for this application brings with it

* Corresponding author. Tel.: +1 406 994 6143; fax: +1 406 994 4452.
E-mail address: kayani@physics.montana.edu (A. Kayani).

0257-8972/$ - see front matter © 2006 Elsevier B.V. All rights reserved.
doi:10.1016/j.surfcoat.2006.02.053

an additional set of problems, namely, guaranteeing the integrity of the coating with respect to adhesion, wear resistance, and detrimental effects associated with interdiffusion between coating and substrate material. On the other hand, using coatings may enable the use of inexpensive alloys that would otherwise be ruled out because of their poor oxidation resistance. The use of coatings to improve oxidation resistance on metal alloys has been known for many years. In our previous work [5], we selected the Cr–Al–N multilayer system for study because it not only offers oxidation resistance at temperatures up to 900 °C [6,7], but also provides wear resistance typical of many metal nitrides [8]. It is known that exposing CrN to oxygen at elevated temperatures leads eventually to loss of nitrogen and formation of Cr_2O_3 [9], a semiconductor with sufficiently low resistivity for the interconnect application at an operating temperature of 800 °C [10]. The oxidation of AlN leads to the formation of Al_2O_3 with unacceptably low conductivity for the interconnect, yet alumina is known to be a good oxidation-resistant barrier. However, if the alumina layer is thin enough we might expect some electronic conductivity coming from electron tunneling or other types of leakage, e.g. through pinholes or layer discontinuities.

In the present work, we have selected coatings from the Cr–Al–O–N system. A variety of nanolayered structures with nanometer-thick layers of alternating chromium oxynitride (CrON) and aluminum oxynitride (AlON) were deposited (see Fig. 1). We expect that by introducing the oxygen during the growth process the Cr containing nanolayer will have mixed phases of Cr_2O_3 and CrN [11,12]. Eventually, the loss of nitrogen during the annealing process will lead to the transformation of the remaining CrN to Cr_2O_3. We expect that the disruption of the coating nanostructure caused by thermal oxide growth will be reduced by introducing the oxygen during film deposition. AlON is a transparent, hard, wear resistant ceramic. Many of its physical properties are similar to those of Al_2O_3, but it has a band gap of only 6.2 eV compared to the 9.9 eV of Al_2O_3 [13]. A smaller band gap will allow for electron tunneling through AlON at lower electric fields than for Al_2O_3. We expect the Al containing oxynitride nanolayer to be composed of mixed phases of AlN and Al_2O_3. Exposing oxygen to the layer at elevated temperatures leads eventually to loss of nitrogen and formation of Al_2O_3. But, if during the annealing process N is retained and stable AlON is formed, the smaller band gap will give a higher conductivity via the electron tunneling process. Moreover, defects in the material will introduce localized states in the band gap that will act as a ladder for the electrons to jump from valance band to conduction band. Finally, because of the rough nature of the substrate due to mechanical polishing, these nanolayers may or may not be continuous. So, in addition to all the processes explained above we expect some electron conduction through pinholes and micro-cracks.

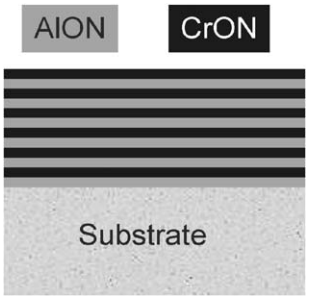

Fig. 1. Schematic diagram of nanolayer structure of the LAFAD coating consisting of AlON and CrON nanolayers.

We used AlON and CrON nanolayers of different bilayer thickness, and grown with different O/N gas ratios, with the goal to study the effect of individual layer thickness and O/N content on oxidation kinetics for the coating. The coatings were deposited on polished 440A steel disks using dual, large-area filtered arc sources [14]. Sample characterization included ion beam analysis for structure and composition of the coatings, atomic force microscopy for surface roughness, and area specific resistance (ASR) for electrical conductivity. The films were annealed at 800 °C in air for up to 25 h, followed by characterization of composition and surface roughness.

2. Experimental procedure

The substrates used for this study were circular disks of 440A steel, 0.75 in. diameter and 0.125 in. thick. The disks were mechanically polished. The nanolayered coatings were deposited by Arcomac Surface Engineering using the Large-Area Filter Arc Deposition (LAFAD) technology with the patented rectangular Large-Area Filtered Arc Source (LAFAS™) that overcomes the limitations of conventional filter designs [14]. The LAFAS™ uses a rectangular plasma-guide chamber with two rectangular deflecting coils installed on opposite sides, as shown in Fig 2. In this design, two primary cathodic arc sources utilizing Cr and Al targets are placed opposite each other on the sidewalls of the plasma-guide chamber, surrounded by rectangular deflecting coils, and separated by an anodic baffle plate. The LAFAS™ vapor plasma source uses superimposed deflecting magnetic fields to turn the metal ion flow 90° toward the deposition chamber and substrates. More massive droplets of material from the source follow straighter trajectories and are captured on baffles, resulting in droplet-free coatings at the substrate. A set of magnetic scanning coils allows the ion plasma jet to be swept in the vertical direction (perpendicular to the plane of Fig. 2) so as to cover theoretically unlimited large surface areas. At the same time, the arc column is well confined by a magnetic field in the horizontal direction, providing enhanced suppression of the turbulent plasma diffusion, and leading to a significant increase in the metal vapor ion yield. By manipulating the arc plasma jets using strategically placed scanning magnetic coils and auxiliary anodes, this novel design creates a “plasma-immersion” environment in the coating chamber. This technique allows the plasma flux from different cathodes in a multi-cathode chamber to be uniformly mixed and to completely envelop complex parts. The use of auxiliary anodes in conjunction with the filtered arc sources permits extraction of a significant electron current from the arc source, which provides a highly conductive ionized gas even without the metal plasma [14].

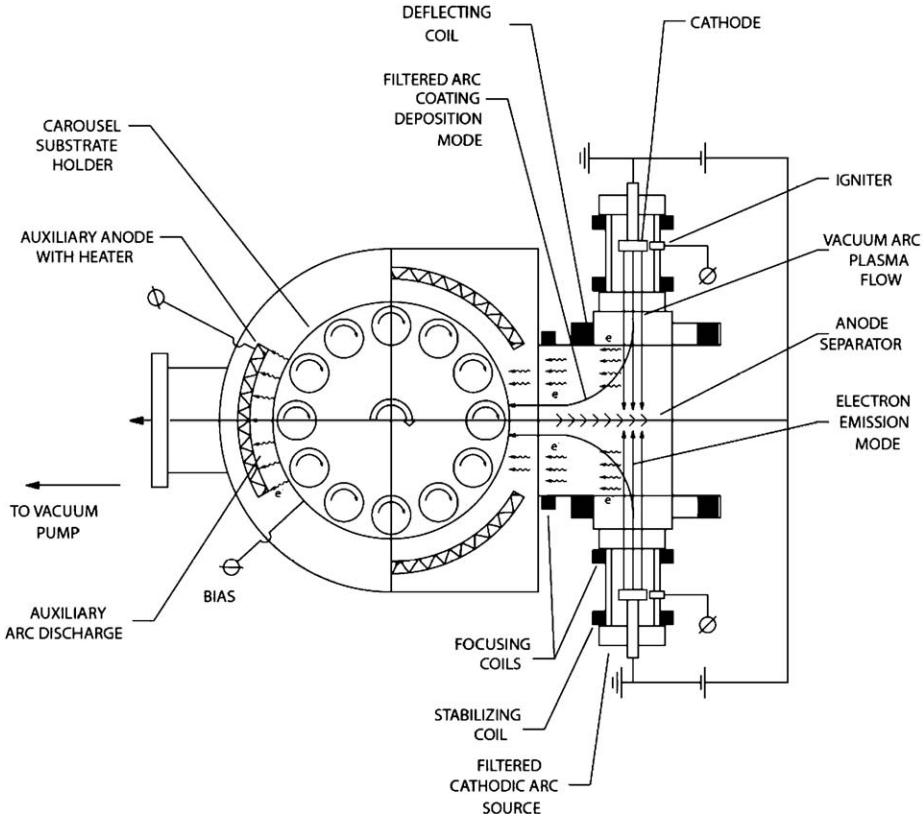

Fig. 2. Schematic drawing of the LAFAD deposition chamber (top view) showing the dual arc sources and sample carousel.

The substrates were mounted on pedestals distributed about the outer rim of a rotating carousel in the chamber. The single rotation process places one surface of the disks in front of the respective Cr or Al sources, once per platform revolution. Thicknesses of the individual layers in the nanolayered structure of the coating were determined by the rotation speed of the carousel in the chamber, either ~3 rpm or ~9 rpm, and were estimated to be either ~4.5 nm or ~1.1 nm, respectively. The substrate temperature during deposition was about 500 °C. The substrates were first cleaned in argon ion plasma with the bias voltage of −250 V at 8×10^{-2} Pa for 20 min, followed by 2 min of −1000 V high voltage Cr ion etching in argon (2×10^{-2} Pa). The Cr and Al ions were deposited in the oxygen and nitrogen atmosphere at 4×10^{-2} Pa with a −50 V bias voltage applied to the sample at a frequency of 50 kHz with a 4 micro-second on time. Oxygen to nitrogen ratios of 1:0, 2:3, 1:4 and 0:1 were chosen for the deposition process. The overall deposition rate was approximately 0.5 μm/h with both the Cr and Al sources running. Overall coating thickness varied, depending on total deposition time and carousel rotation speed. The coatings considered here are listed in Table 1. Sample names in the first column of the table represent the composition of the sample and the rotation speed of the carousel. For example, sample A3 represents CrO/AlO coating with a carousel rotation speed of 3 rpm. The unit of thickness in column 3 (10^{15} atoms/cm^2) is a measure of areal atomic density determined in ion beam analysis, and can be converted to a thickness by dividing by the material density. In this case, the coating density is not known, but a very rough estimate of coating thickness can be obtained by assuming that 10^{15} atoms/cm^2 corresponds to about 0.2 nm.

Oxidation of the samples was carried out using a standard tube furnace operated horizontally in air, with no additional fixtures to control humidity or flow rate. Samples were mounted vertically in a ceramic cassette at the center of the horizontal furnace tube. The oven temperature was controlled electronically with a 30-min rise time to 800 °C. Soak times were incremented to give total oxidation periods of 1, 4, 9, and 25 h. After each increment of oxidation time, the oven was cooled over a period of 30 min. The samples were removed and placed in the vacuum chamber for ion beam analysis. Surface

Table 1
Structure parameters of CrON/AlON coatings on 440A steels

Sample	Sample description	Oxygen/nitrogen	Approximate thickness 10^{15} atoms/cm^2
A3	CrO/AlO	1:0	5150
A9	CrO/AlO	1:0	–
B3	CrON/AlON	2:3	11,650
B9	CrON/AlON	2:3	12,100
C3	CrON/AlON	1:4	13,750
C9	CrON/AlON	1:4	11,950
D3	CrN/AlN	0:1	14,950
D9	CrN/AlN	0:1	9550

microscopy was performed prior to oxidation, and at the end of the 25-h oxidation period.

3. Results and discussion

Fig. 3 shows atomic force microscopy (AFM) images recorded in tapping mode after deposition of the coatings (left column) and again after 25-h oxidation at 800 °C in air (right column) for samples A3, B3, C3 and D3. The lateral width for each image is 5 μm and the image locations are not the same for a given sample. It can be seen that all the as-deposited coatings are smooth on a submicron scale. The rms roughness in the as-deposited coatings is in the range of 32–50 nm which indicates that the individual nanolayers might not be continuous. After oxidation, the rms roughness for samples A3, B3 and C3 has not changed although the surface appears to have a more fine-grain texture. The most noticeable change following oxidation occurs for sample D3. The roughness increases by an order of magnitude from 15 nm to 115 nm, and the surface is characterized by large nodules. Based on results (below) from the RBS analysis, we conclude that these nodules probably correspond to clusters of Fe oxide. Diffusion of Fe to the surface of this coating is observed in RBS, and may be an indication of cracking or other forms of degradation of this CrAlN coating following the 25-h oxidation at 800 °C.

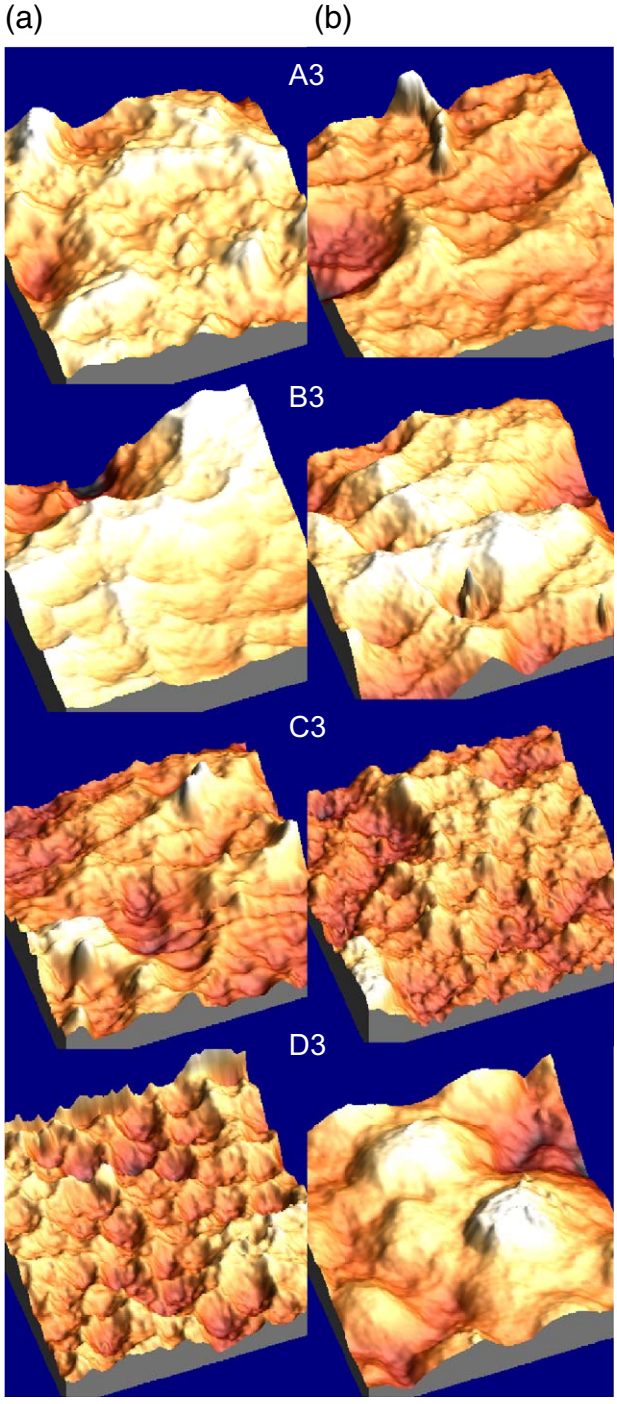

Fig. 3. AFM images of four nanolayer coatings before (left column) and after (right column) oxidation in air for 25 h. Each image has a lateral size of 5 μm.

Ion beam analysis of the samples was performed using the 3 MV tandem accelerator at the Environmental Molecular Sciences Laboratory (EMSL) at Pacific Northwest National Laboratory (PNNL) in Richland, WA. Rutherford backscattering spectra (RBS) were recorded using a 4.0 MeV beam of He^+ ions with a 60° angle of incidence measured from the sample normal. Backscattered ions were collected using a silicon surface barrier detector at a scattering angle of 165°, with an exit angle of 45° from the sample normal. This geometry enhanced the depth resolution of the RBS measurements. Spectra were collected after total oxidation periods of 1, 4, 9 and 25 h at 800 °C. The samples were removed from the oven for ion beam analysis, and were thus subjected to some thermal cycling that might have adversely affected the coatings. Composition profiles were determined by comparing SIMNRA computer simulations of the spectra with the original data [15]. Since the depth resolution of RBS with these beam parameters and detectors is larger than 15 nm, we did not attempt to simulate individual layers in the coating, but rather divided the sample up into the minimum number of layers needed to give a reasonable fit to the spectrum. The composition profiles determined in this way are shown in Fig. 4 for the as-deposited samples A3, B3, C3 and D3, prior to oxidation. The depth scale (10^{15} atoms/cm^2) is characteristic of the RBS measurement, which only determines the number of target atoms per cm^2 visible to the analysis beam. If the sample density is known, this scale is readily converted to a linear depth scale. However, roughly we can take 1×10^{15} atoms/cm^2 to be one layer of atoms, or approximately 0.2 nm. The vertical scale is a percentage concentration, based on the assumption that the individual concentrations add to 100%. No measurement of hydrogen concentration was made for these coatings, so the percentages are normalized to the four elements shown in the coatings.

Rutherford backscattering is particularly useful for obtaining concentration depth profiles for the heavier elements in the coating, but is somewhat limited in detecting the light elements such as O and N because of the quadratic dependence of the Rutherford cross section on the atomic number of the target atom. Nuclear reaction analysis (NRA) can be quite useful in this case because the spectral peaks typically sit on a very low or zero-background signal [16]. A limitation for NRA is that

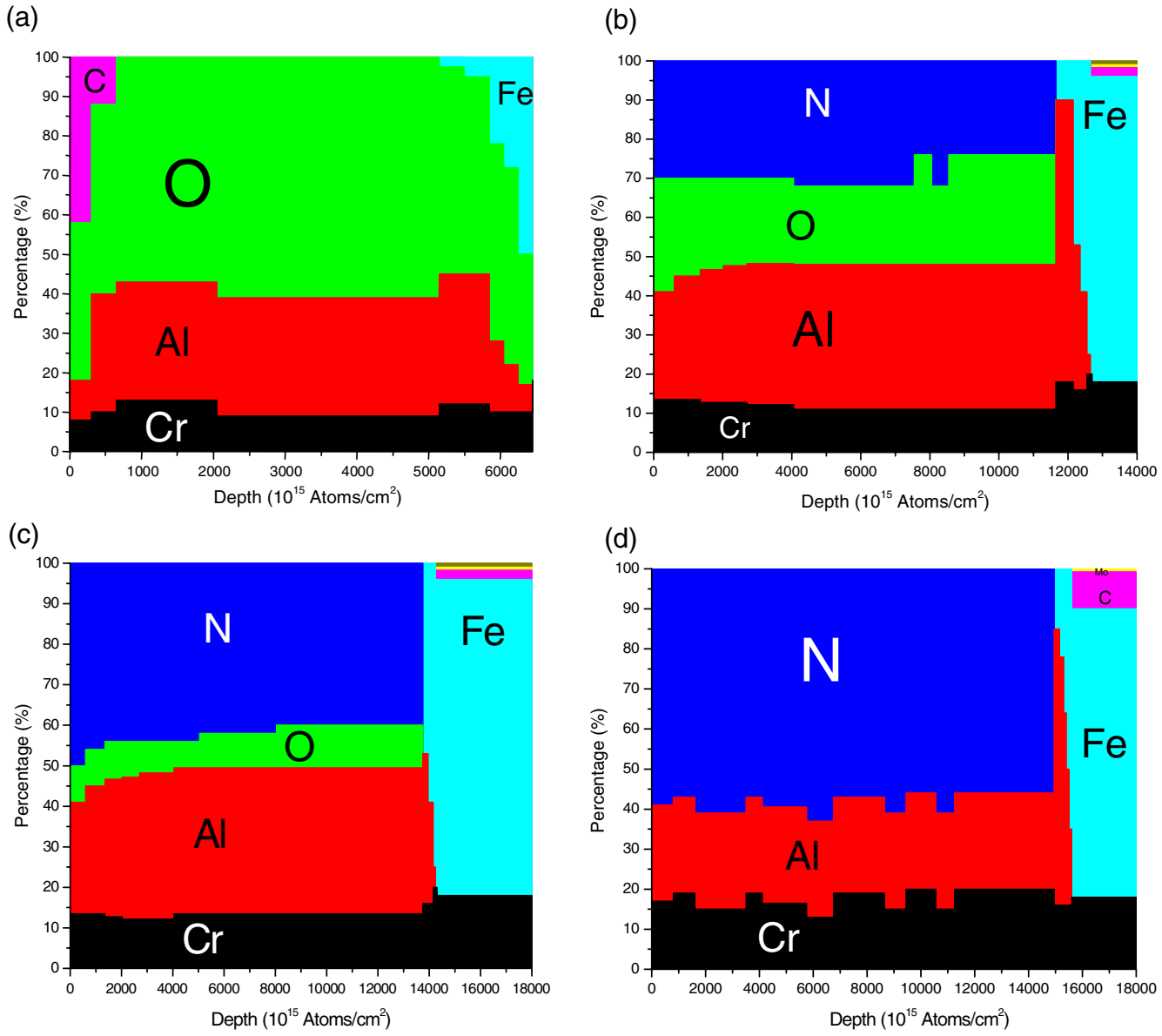

Fig. 4. Composition profile of as-deposited coatings (a) A3, (b) B3, (c) C3, (d) D3.

the reaction cross sections are generally known only for a few selected scattering angles, and thus may need to be measured using standard thin films of known stoichiometry. For the present measurements a beam of 1.0 MeV deuterium ions (d^+) was incident on the samples at an angle of 60° from the surface normal. Reaction products were detected at a scattering angle of 170°, 50° from the sample normal. A thin aluminized mylar film covered the detector to stop backscattered deuterium ions, allowing only the more energetic reaction products to enter the detector. The detected particles for these measurements were protons from the $^{14}N(d,p)^{15}N$ and $^{16}O(d,p)^{17}O$ reactions. The reaction cross sections for our experimental geometry were determined in a separate experiment using commercially prepared films of Si_3N_4 and SiO_2 with known thickness. Peak areas from the measured yields were converted to N or O concentrations. Since the depth resolution when using these particular reactions is not nearly as good as that for the RBS measurements, our primary purpose for using NRA was to determine the total N and O concentrations in the coatings as a function of annealing time. These total concentrations were then compared with the total concentrations determined from the RBS measurements. The set of target composition profile parameters was adjusted until a single set of parameters could be used to accurately simulate both the RBS and NRA measurements using the SIMNRA program. In some cases there is a rapid decrease in N content following the initial 1-h heat treatment, attributed to the transformation of CrN to Cr_2N [9,17]. A more gradual loss of N during subsequent annealing is attributed to the transformation of Cr_2N to Cr_2O_3. The total N content varies from sample to sample because of the different nanolayer structures and coating preparation conditions.

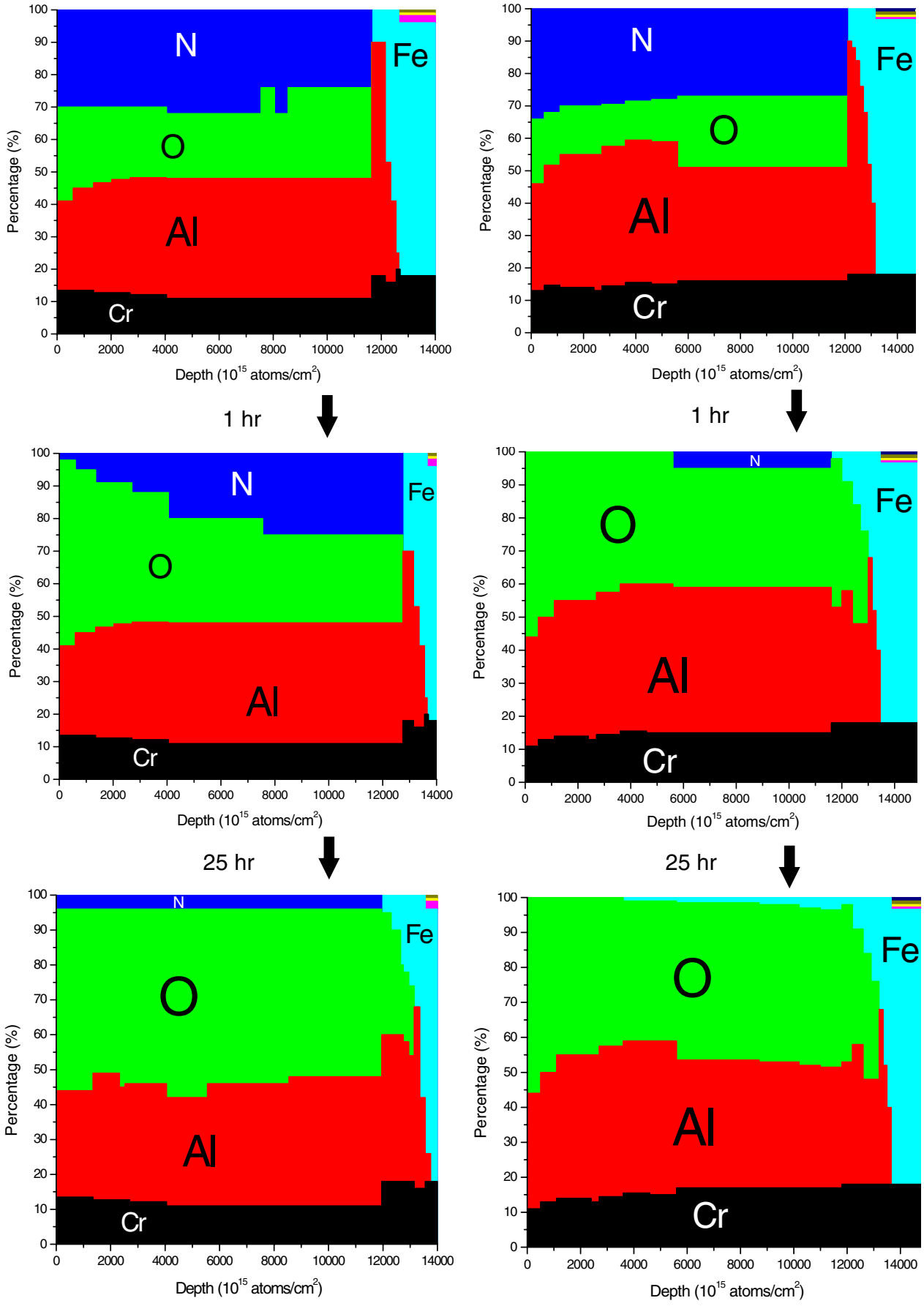

Fig. 5. Composition profile evolution with annealing for sample B3 (left column) and sample B9 (right column).

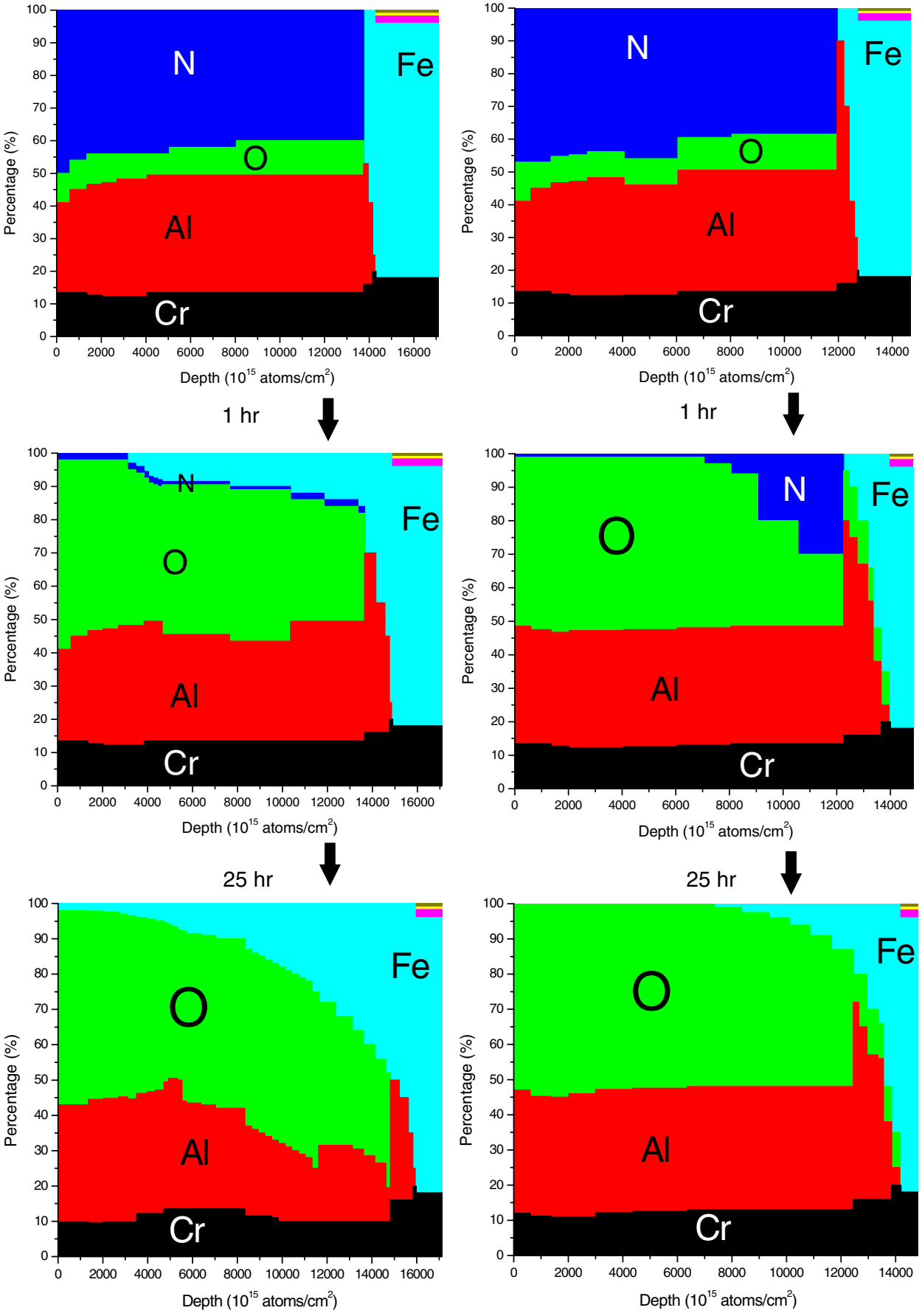

Fig. 6. Composition profile evolution with annealing for sample C3 (left column) and sample C9 (right column).

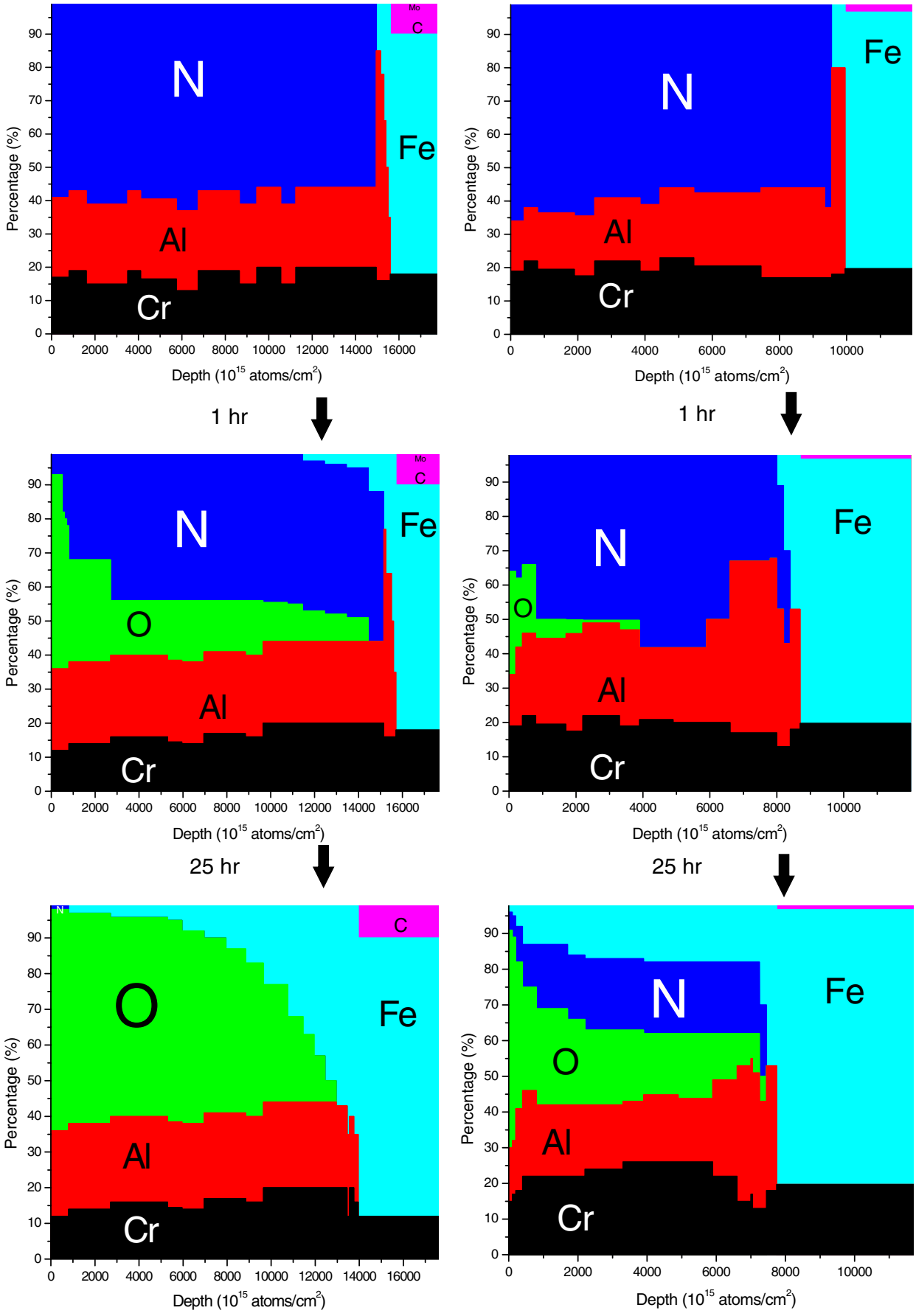

Fig. 7. Composition profile evolution with annealing for sample D3 (left column) and sample D9 (right column).

The survey of the as-grown coatings deposited with 3 rpm, presented in Fig. 4, shows that the incorporation of oxygen in the samples during growth is in accordance to the ratio of oxygen to nitrogen in the chamber during the growth process. For example the oxygen concentration in sample B3, deposited with the oxygen to nitrogen ratio of 2:3, is greater than that for sample C3, for which this ratio was 1:4. Similarly no oxygen is found in the sample D3, grown with a pure nitrogen atmosphere. Similar behavior was observed in the coatings deposited with a carousel rotation speed of 9 rpm.

The coatings analyzed here behave very differently when subjected to the high-temperature oxidizing atmosphere. Sample A3, with only oxygen in the growth chamber, survived the high-temperature oxidation relatively unchanged. After 25 h of heating the composition remained unchanged, and no interdiffusion of heavier elements between the substrate and coating was observed. However, a small percentage of carbon was observed on the surface that was not found in the 1-h heated sample. This sample was non-conducting, and was therefore removed from the batch of samples for analysis.

Sample B3 contained approximately 20% oxygen as grown (Fig. 5, left column). Complete oxidation occurred with heating at 800 °C, as oxygen gradually replaced the nitrogen in the coating. After 25 h at 800 °C, less than 5% nitrogen is left in the sample. However, sample B9, which has a thinner bilayer than sample B3, lost almost all of the nitrogen in only 1 h of heating (Fig. 5, right column). Negligible diffusion of substrate elements (primarily Fe) into the coating was observed in the case of sample B3. However, in the case of B9 a small percentage of Fe is found to have diffused into the coating, but it did not diffuse all the way to the surface after 25 h. Based on the results below for coatings with less oxygen, we conclude that introducing oxygen during the coating growth process creates more effective diffusion barriers that stop, or at least slow down the diffusion of Fe from the substrate into the coating. Oxidation of the coatings leads to the formations of Cr_2O_3 and Al_2O_3, which is evident from the stoichiometry obtained by RBS for these compounds (Fig. 5, bottom).

Coating C3 contains about 10% oxygen concentration as grown (Fig. 6, top). In marked contrast to sample B3, the nitrogen in sample C3 is almost completely replaced by oxygen after only 1 h of heating at 800 °C, and is seen to be susceptible to Fe diffusion from the substrate to the coating surface after only a few hours in the oven (Fig. 6, left column). In coating C9 the nitrogen loss behavior is almost the same as observed for coating C3, but the Fe diffusion from the substrate is considerably slower than for sample C3. In sample C9, Fe was not yet seen on the surface after 25 h of heating (Fig. 6, right column).

For coating D3 there is no oxygen in the as grown sample. The nitrogen in the coating is gradually replaced by oxygen, and is completely lost after 25 h of heating at 800 °C (Fig. 7, left column). Diffusion of Fe into the coating begins after only 1 h of heating, and Fe has reached the surface of the coating after 25 h of heating. Diffusion of Fe from the substrate to the coating surface was also seen in coating D9, and appears to be greater than that found for sample D3. The performance of coatings D3 and D9 appears to be not nearly as good as that for samples studied previously [5]. The primary difference between these two processes is in the rotation of the substrate in front of the Cr and Al sources (double vs. single rotation). Contrasting the properties of coatings grown with these two rotation modes is currently under investigation.

The area specific resistivity (ASR) for uncoated and coated samples has been investigated. The ASR values for both coated and uncoated samples reached a minimum of below 10 $m\Omega\ cm^2$. However, the ASR value of the uncoated sample rose relatively fast compared to that for the coated sample, indicating reduced oxidation rate and increased electrical conductivity for the coated samples. Moreover, SEM analysis has shown that the oxide scale on the uncoated samples is significantly thicker than that for the coated samples after 1000 h of annealing at 800 °C in air. Results of this investigation have been published elsewhere [18].

The most likely mechanism of oxide formation for the nanolayers is the loss of N from the CrN as it transforms to Cr_2N at the high temperature, and the replacement of N by O in forming Cr_2O_3 in the nanolayers [9,17]. Results similar to these were reported for high-temperature oxidation of CrN films on steel [19]. In those experiments, XPS depth profiles show that in addition to the transformation from CrN to Cr_2O_3, Fe oxide is formed at the surface as Fe diffuses from the steel substrate out through the CrN coating. Enhanced diffusion can occur at higher temperatures. Also the mismatch in the thermal expansion coefficients between substrate and coating results in film stress, cracking and loss of adhesion at the coating/substrate interface. It appears that the presence of oxygen in the as-deposited nanolayered coatings reduces the amount of Fe diffusion from the substrate.

4. Summary

In summary, we report results for the high-temperature oxidation resistance of the 440A steel alloy with a coating consisting of stacked CrON and AlON nanolayers. The results from ion beam analysis are quantitative and can be used to show either total oxygen content or oxide thickness as a function of time. Ion beam analysis shows that oxidation rates can be greatly reduced with these coatings, and point to a nanolayered structure with sub-nm layer thickness as showing good performance for periods of up to 25 h at 800 °C in air. Future measurements will extend the annealing time to better simulate the interconnect application in a solid oxide fuel cell.

Acknowledgements

We acknowledge the technical assistance of Norm Williams and John Getty at Montana State University. Microscopy (AFM) was performed at ICAL, located at Montana State University. Ion beam analysis was performed at the EMSL, a national scientific user facility located at PNNL and supported by the U.S. Department of Energy's Office of Biological and Environmental Research. PNNL is a

multi-program national laboratory operated for the U.S. DOE by Battelle Memorial Institute under contract No. DE-AC06-76RLO 1830. Work at MSU was supported through the High-Temperature Electrochemisty Center (HiTEC) supported by a DOI and DOE subcontract from PNNL, number 3917 (413060-A).

References

[1] B.C.H. Steele, A. Heinzel, Nature 414 (2001) 345.
[2] Z.G. Yang, J.W. Stevenson, P. Singh, Adv. Mater. Process. 161 (2003) 34.
[3] Z. Yang, K.S. Weil, D.M. Paxton, J.W. Stevenson, J. Electrochem. Soc. 150 (2003) A1188.
[4] http://www.thyssenkrupp.com/en/presse/art_detail.html&aid=931&oid=930.
[5] R.J. Smith, C. Tripp, A. Knospe, C.V. Ramana, A. Kayani, Vladimir Gorokhovsky, V. Shutthanandan, D.S. Gelles, J. Mater. Eng. Perform. 13 (2003) 295.
[6] M. Kawate, A.K. Hashimoto, T. Suzuki, Surf. Coat. Technol. 165 (2003) 163.
[7] O. Banakh, P.E. Schmid, R. Sanjines, F. Levy, Surf. Coat. Technol. 163–164 (2003) 57.
[8] S. PalDey, S.C. Deevi, Mater. Sci. Eng., A Struct. Mater.: Prop. Microstruct. Process. 342 (2003) 58.
[9] F.-H. Lu, H.-Y. Chen, C.-H. Hung, J. Vac. Sci. Technol., A, Vac. Surf. Films 21 (3) (2003) 671.
[10] K. Huang, P.Y. Hou, J.B. Goodenough, Mater. Res. Bull. 36 (2001) 81.
[11] St. Collard, H. Kupfer, G. Hecht, W. Hoyer, H. Moussaoui, Surf. Coat. Technol. 112 (1999) 181.
[12] C. Gautier, J. Machet, Surf. Coat. Technol. 94–95 (1997) 422.
[13] Encyclopedia of Materials, Elsevier Science Ltd, 2001, p. 127.
[14] V.I. Gorokhovsky, R. Bhattacharya, D.G. Bhat, Surf. Coat. Technol. 140 (2001) 82.
[15] M. Mayer, SIMNRA User's Guide, Technical Report IPP 9/113, Max-Planck-Institut fur Plasmaphysik, Garching, Germany, (1997).
[16] J.R. Tesmer, M. Nastasi, Handbook of Modern Ion Beam Materials Analysis, Materials Research Society, Pittsburgh, PA, 1995.
[17] H.-Y. Chen, F.-H. Lu, J. Vac. Sci. Technol., A, Vac. Surf. Films 21 (3) (2003) 695.
[18] P.E. Gannon, C.T. Tripp, A.K. Knospe, C.V. Ramana, M. Deibert, R.J. Smith, V.I. Gorokhovsky, Surf. Coat. Technol. 188–189 (2004) 55.
[19] I. Milosev, J.M. Abels, H.-H. Strehblow, B. Navinsek, M. Metikos-Hukovic, J. Vac. Sci. Technol., A, Vac. Surf. Films 14 (4) (1996) 2527.